Optical Engineering

OpticalEngineering.SPIEDigitalLibrary.org

Aspheric lens mounting

Frédéric Lamontagne
Ulrike Fuchs
Martin Trabert
Anna Möhl

SPIE.

Frédéric Lamontagne, Ulrike Fuchs, Martin Trabert, Anna Möhl, "Aspheric lens mounting," *Opt. Eng.* **57**(10), 101708 (2018), doi: 10.1117/1.OE.57.10.101708.

Aspheric lens mounting

Frédéric Lamontagne,[a,*] Ulrike Fuchs,[b] Martin Trabert,[b] and Anna Möhl[b]
[a]INO, Québec, Quebec City, Canada
[b]Asphericon GmbH, Jena, Germany

Abstract. Mounting aspheres is often challenging because of the higher sensitivity to decenter and tilt compared with spherical lenses. This paper first describes aspheric surface decenter and tilt error as per ISO 10110 standard. Then, the most common lens mounting and alignment method for aspheric lenses are discussed in detail. Finally, an innovative mounting method that uses surface contact mounting is presented. This autocentering method uses the optical surfaces as mounting interfaces to provide a high level of centering accuracy for aspheric lenses. Centering measurement results for different aspheric lenses mounted using this method are also presented. [DOI: 10.1117/1.OE.57.10.101708]

Keywords: lens mounting; asphere; aspheric lens; alignment; autocentering; centering.

Paper 180160SSP received Jan. 29, 2018; accepted for publication Jul. 24, 2018; published online Aug. 17, 2018.

1 Introduction

The quality of an optical system strongly depends on the alignment accuracy of the optical elements composing it. As a result, the mounting of the optical elements shall be done to minimize the centering, the tilt, and the axial positioning errors with respect to the nominal optical layout. A lens can be considered to be perfectly aligned when its optical axis is coincident with the optical system reference axis. The optical axis of a spherical lens corresponds to the line connecting the two centers of curvature. In the case of a lens having a planar surface, the optical axis of the lens is the line perpendicular to the planar surface and passing through the center of curvature of the spherical surface. Unlike the spherical surface, which is fully described by its radius and the position of its center of curvature, the description of an aspheric surface is not complete without the definition of its axis of symmetry. As per ISO 10110 standard,[1,2] aspheric surface centering tolerances are specified as the distance between the aspheric surface center point and the lens reference axis, and by the tilt angle of the aspheric surface axis with respect to the lens reference axis. The aspheric surface center point is the point where the aspheric surface axis intersects the aspheric surface as shown in Fig. 1.

In addition to the optical surfaces, lenses are most of the time also composed of mechanical surfaces that have no optical function such as outer cylinder surface, flat surface, or chamfers. These mechanical surfaces can be used as mounting interface, to eliminate sharp and brittle features, or simply to remove unnecessary material to reduce size and mass.

Part 6 of ISO 10110 specifies rules to indicate datum axis and centering tolerances for optical elements. For aspheric lens, the ISO 10110 drawing indication code $4/\sigma(L)$ is used for indicating the tolerable manufacturing error of the aspheric surface with respect to the datum axis. The symbol σ is the maximum permissible tilt in arc min or arc sec, and L is the maximum lateral displacement of the center point from the datum axis in mm. In the example of Fig. 2(a), the datum axis is perpendicular to plane A and pierces the central point of the right surface. Figure 2(b) shows the aspheric lens of Fig. 2(a) with exaggerated manufacturing error. The aspheric surface is decentered of 0.2 mm and tilted of 2 arc min with respect to the lens reference axis defined by datum A and datum B.

In opposition to spherical lens, the manufacturing error between the aspheric surface and the second optical surface of the lens cannot be compensated by further alignment of the lens. In the example of Fig. 2, the tilt error between the optical axis of the aspheric surface and the planar optical surface will remain regardless of the mounting and alignment methods. Thus, the manufacturing error of the optical element itself shall be toleranced carefully as it cannot be completely corrected by alignment.[3]

2 Aspheric Lens Mounting

As for spherical lenses, common aspheric lens mounting and alignment methods can be divided in two main categories: the drop-in assembly and the active alignment. In the drop-in assembly, the lens is simply dropped into the barrel and secured with a retainer. Stepped barrel that can accommodate different lens diameters and assembly with spacer between lenses having the same diameter are two similar implementations of the drop-in. The centering error of a lens mounted using the drop-in method is most of the time controlled by the radial clearance between the lens and the barrel bore diameter. Therefore, the tolerances on lens diameter, barrel bore diameter, and on the centration of the lens rim with respect to the lens optical axis all contribute to the lens centering error once mounted in the barrel. Figure 3 shows the aspheric lens of Fig. 2 mounted in a barrel using the drop-in technique. The planar optical surface (lens datum A) is used to mount the lens on the barrel seat. The centering error of the lens is constrained by the lens rim (lens datum B). In this example, the centering error of the center point of the aspheric surface is the sum of the aspheric surface lateral displacement from the lens manufacturing error and the radial clearance between the lens outside diameter (OD) and the barrel inside diameter (ID). The tilt is the

*Address all correspondence to: Frédéric Lamontagne, E-mail: frederic.lamontagne@ino.ca

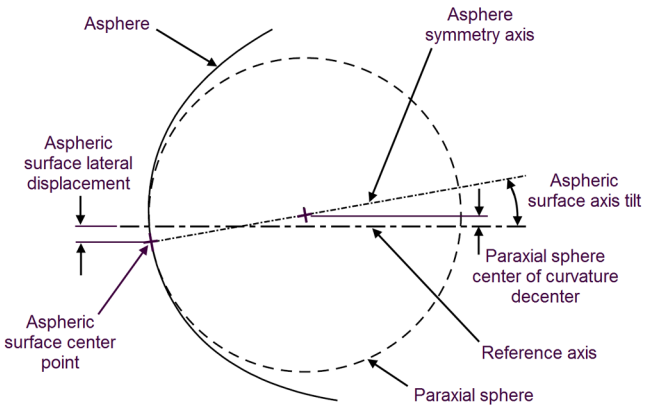

Fig. 1 Aspheric surface optical axis.

sum of the aspheric optical axis tilt from the lens manufacturing, and the tilt of the barrel mounting interface with respect to the barrel reference axis. Most of the time, measurement of the positioning error of an aspheric surface is accomplished by measuring the centering error of the paraxial sphere center of curvature and the tilt of the aspheric surface optical axis with respect to the barrel reference axis. In this case, the centering error of the paraxial sphere center of curvature should include all the centering errors listed above added to the effect of the aspheric optical axis tilt.

The drop-in is a method that is quite simple to implement. However, when the centering accuracy requirements are more stringent, such as it is often the case for aspheric lens, tight manufacturing tolerances are needed. As the tolerance precision increases, the manufacturing cost also increases. When the centering requirement is too difficult or too expensive to achieve with the drop-in mounting method, an active alignment is required. A common method used for aspheric lens alignment is to align the paraxial sphere center of curvature on the barrel reference axis. The measurement of the paraxial sphere shift can be done as for spherical surface using an autocollimator. In the example of Fig. 4, the lens is mounted in the barrel on a precision seat that constraints the axial position of the lens and the tilt of the planar surface. The lens is then translated and bonded in the barrel so that the paraxial sphere center of curvature is centered on the barrel reference axis. The tilt manufacturing error between the aspheric surface optical axis and the planar optical surface can unfortunately not be compensated, hence the importance of a good control of the manufacturing error of the aspheric surface. Depending on the design constraints, the lens can be centered and glued in a subcell, and then stacked in a main barrel. In other implementation, the lens can be centered and glued directly into the main barrel.

If the lens surface in contact with the barrel is spherical instead of planar, the lens rolls around its spherical surface center of curvature during the alignment rather than

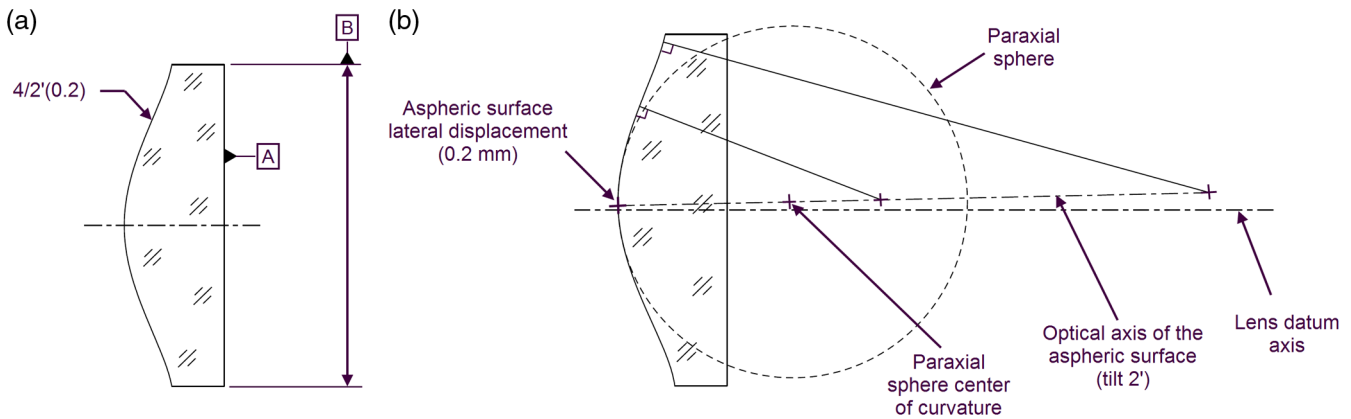

Fig. 2 Aspheric lens tolerancing. (a) Nominal lens and (b) exaggerated lens decenter and tilt manufacturing errors.

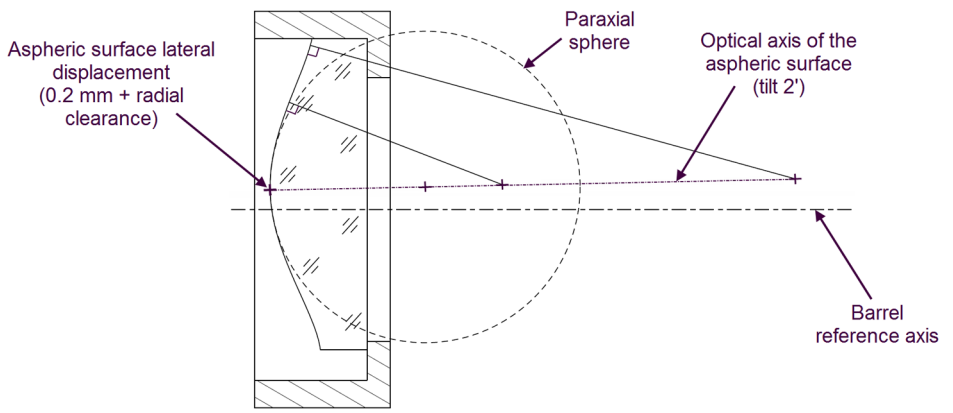

Fig. 3 Aspheric lens drop-in assembly.

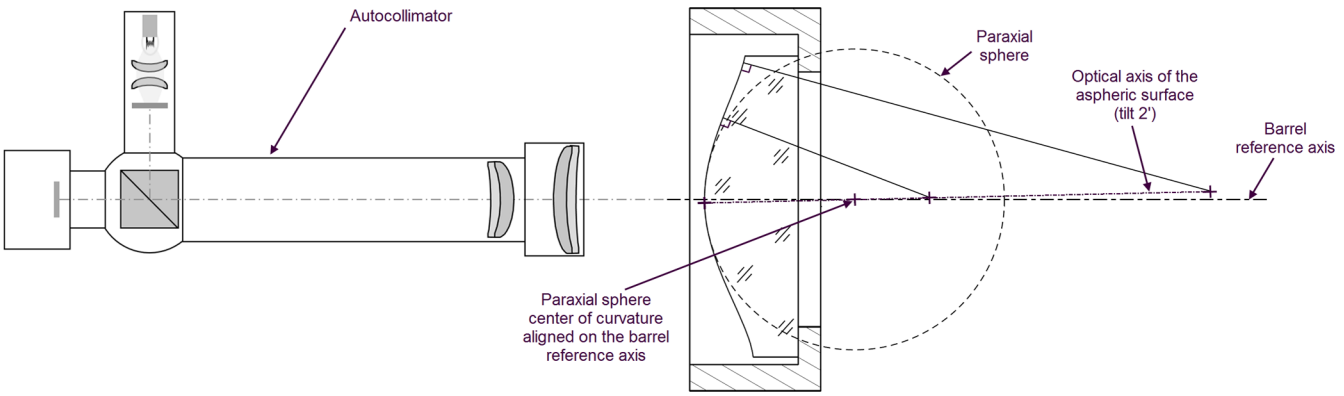

Fig. 4 Aspheric lens active alignment.

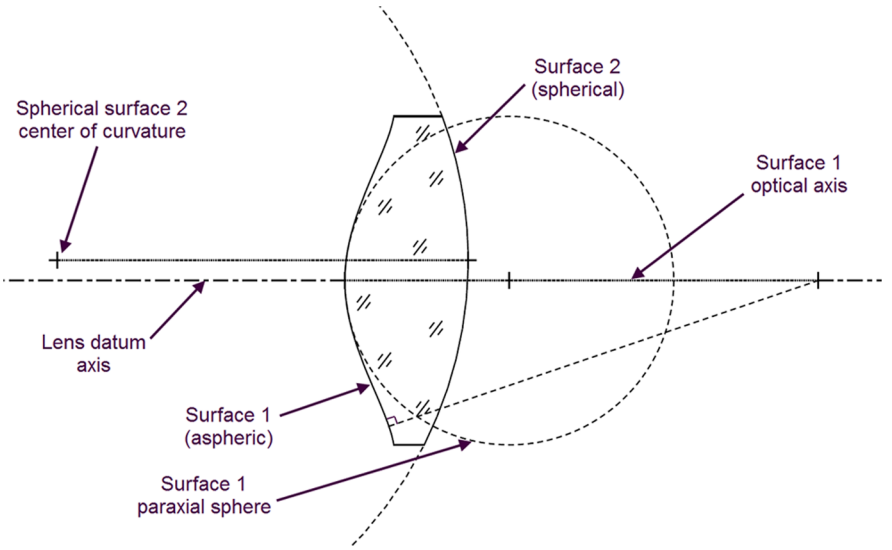

Fig. 5 Aspheric-spherical lens with exaggerated manufacturing error.

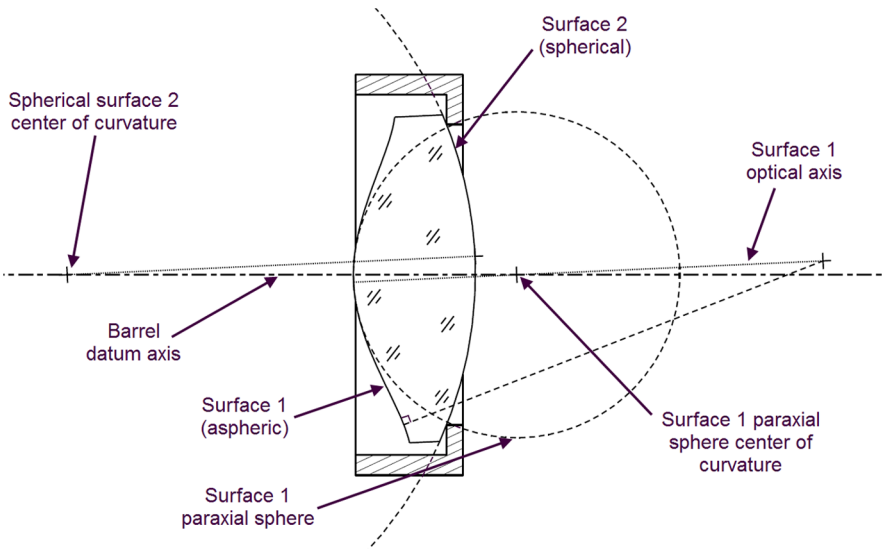

Fig. 6 Aspheric-spherical lens active alignment.

translates. The position of the spherical surface interfacing with the barrel is constrained by the precision seat on the barrel, providing a self-centering for the spherical surface. The alignment is done on the lens aspheric surface that is opposite to the barrel seat. Because of the inevitable manufacturing error of the lens, the spherical surface center of curvature will be decentered with respect to the aspheric surface axis as shown in Fig. 5. As a result, the alignment of the lens in the barrel that is performed on the aspheric surface paraxial sphere center of curvature will induce a tilt error on the aspheric axis with respect to the barrel reference axis as shown in Fig. 6. In the case of an aspheric surface interfacing with the barrel seat, the lens rolls around the local radius of curvature at the barrel seat interface.

3 Aspheric Lens Autocentering

A new lens mounting method that bridges the simplicity of the drop-in with a centering accuracy close to the active alignment has been developed recently. This method, called autocentering, is based on surface-contact lens mounting. With this mounting method, the lens is clamped directly on the optical surfaces between the barrel seat and a special threaded ring. As the autocentering uses surface-contact mounting, the clamping angle at the lens mounting interface needs to be large enough to overcome the friction force to allow the self-centering of the lens.[4] The following description provides an introduction to the autocentering principle.

To appropriately define a lens centering error with respect to the barrel reference axis, both lens surfaces need to be considered. It has been shown that very good centering accuracy, generally <0.3 arc min, can be expected for a spherical optical surface mounted directly on a barrel seat with the drop-in method.[5] On the other hand, centering error as high as 5 arc min has been observed for the second optical surface centered using surface-contact mounting with standard threaded ring. In such cases, the centering error of the lens surface in contact with the threaded ring depends on the positioning errors of the ring lens seat.[6,7] More precisely, the two factors that affect the centering error of the lens surface in contact with the threaded ring are the ring centering error and the ring tilt error with respect to the barrel reference axis.[4] The centering error of the threaded ring comes from the assembly clearance between the ring and the barrel threads. For its part, the tilt error of the threaded ring comes from the combination of the thread angle and the ring decenter from the assembly clearance in the threads. To have a good understanding on how the thread angle affects the ring tilt error, we need to be aware that the ring thread is constrained by its top thread surface within the barrel thread. In fact, when a ring is rotated to secure a lens in a barrel, an axial force constrained the lens on the barrel seat and a reaction force pushes the ring on the opposite side so that the ring is constrained by its top thread surface as shown in Fig. 7. As a result, the tilt of the threaded ring is a function of the thread angle and the ring decenter as shown in Fig. 8. It is interesting to note that, in the case of the lens of Fig. 8, the ring tilt effect on the lens centering error is larger than the ring decenter effect as the lens and the ring are decentered in opposite directions.

To overcome the lens centering error caused by standard threaded ring for surface-contact lens mounting, it is possible to adjust the thread angle to meet an autocentering condition for the lens to be assembled. When the autocentering condition is met, the ring decenter and the ring tilt have counterbalancing effect on the lens centering. This means that the ring decenter acts on the lens centering in one direction and that the ring tilt acts on the lens centering in the opposite direction in the same magnitude, providing a self-alignment on the lens. Therefore, the lens is maintained aligned independently of the ring positioning error. The thread angle to meet the autocentering condition for a given lens geometry is defined by the following equation:

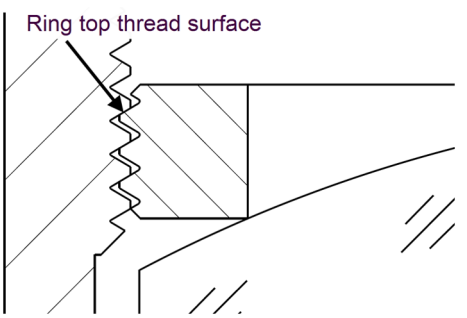

Fig. 7 Threaded ring constrained by the top thread surface.

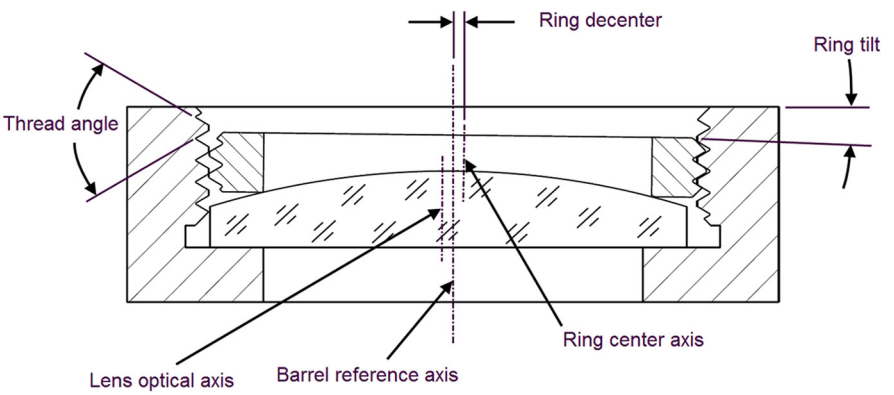

Fig. 8 Relationship between the ring decenter and ring tilt.

$$\varphi_{\text{threads}} = 2\tan^{-1}\left(\frac{d_{\text{ring}}}{2\sqrt{R^2 - Y^2} + 2h + T}\right), \tag{1}$$

where d_{ring} is the major diameter of the retaining ring, R is the radius of curvature of the lens surface in contact with the retaining ring, Y is the half-diameter of the retaining ring's clear aperture, h is the distance between (i) the first point of contact of the barrel threads with the ring threads next to the optical element and (ii) the point of contact of the retaining ring with the peripheral region of the second surface, and T is the distance between (i) the first point of contact of the barrel threads with the ring threads next to the optical element and (ii) the last point of contact of the barrel threads with the ring threads farthest from the optical element diametrically opposite to the first point of contact.

The autocentering condition parameters involved in Eq. (1) are shown in Fig. 9. Figure 10 shows an example of a lens that is centered using the autocentering principle. It can be seen that the retaining ring is constrained by the top thread interface and that the ring is decentered and tilted. However, even if the ring has a positioning error, the lens is still centered on the barrel reference axis as the autocentering condition is met.

Experimental measurements have demonstrated that the autocentering method results in centering errors of the lens surface in contact with the ring, which are typically in the order of 0.5 arc min for spherical surface. If we express this centering error in terms of decenter instead of tilt following the relationship decenter = sin (tilt) * radius, this corresponds to centering error generally <5 μm for lens having diameters ranging from 5 to 50 mm.

For aspheric lens, the same principle can be applied with the difference that the local radius of curvature at the ring interface diameter is used in Eq. (1). To compute this local radius of curvature, we start with the aspheric surface description given as

$$z(r) = \frac{r^2}{R\left[1 + \sqrt{1 - (1+k)\frac{r^2}{R^2}}\right]} + \sum_{i=2}^{n} A_{2i} r^{2i}, \tag{2}$$

where $z(r)$ is the sagitta of the aspheric surface at distance r from the symmetry axis, r is the radial distance from the optical axis, R is the paraxial surface radius, k is the conic constant, and A is the aspheric coefficient.

The derivative of the aspheric function gives the slope of the tangent line to the aspheric surface at the radial distance r from the axis of symmetry. The local radius of curvature at the radial distance r from the symmetry axis to be used in the autocentering thread angle calculation is computed with Eq. (3)

$$R_r = \frac{r}{\sin\left\{\tan^{-1}\left[\frac{d}{dr} z(r)\right]\right\}}. \tag{3}$$

The expanded form of the aspheric function [Eq. (2)] for the first seven aspheric terms is

$$z = \frac{r^2}{R\left[1 + \sqrt{1 - (1+k)\frac{r^2}{R^2}}\right]} + A_4 r^4 + A_6 r^6 + A_8 r^8 + A_{10} r^{10} + A_{12} r^{12} + A_{14} r^{14} + A_{16} r^{16}. \tag{4}$$

Thus, the derivative of the aspheric function used in the computation of the local radius of curvature in Eq. (3) is given as

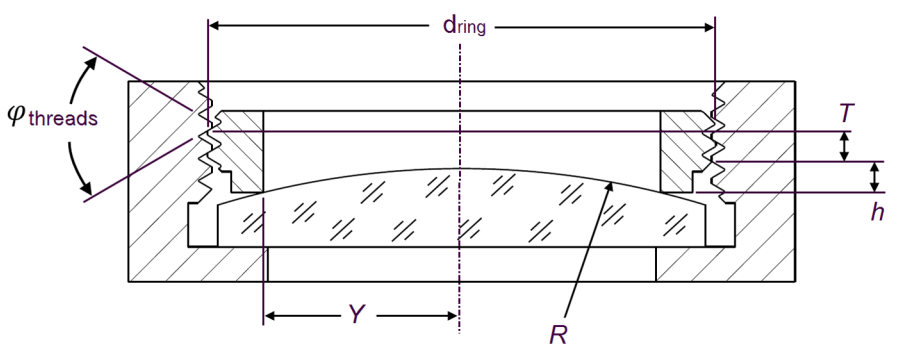

Fig. 9 Autocentering condition parameters.

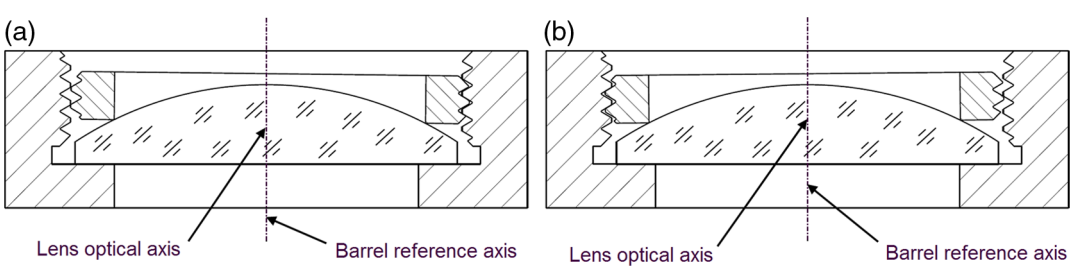

Fig. 10 Autocentered lens not affected by the ring centering error. (a) Threaded ring decentered on the right side, (b) threaded ring decentered on the left side.

$$\frac{d}{dr}z(r) = 4A_4r^3 + 6A_6r^5 + 8A_8r^7 + 10A_{10}r^9 + 12A_{12}r^{11} + 14A_{14}r^{13} + 16A_{16}r^{15} + \frac{2r}{R\left[\sqrt{1-\frac{r^2(k+1)}{R^2}}+1\right]} + \frac{r^3(k+1)}{R^3\left[\sqrt{1-\frac{r^2(k+1)}{R^2}}+1\right]^2\sqrt{1-\frac{r^2(k+1)}{R^2}}}. \quad (5)$$

Equation (6) is the combination of Eqs. (1) and (3). Using the derivative of the aspheric function Eq. (5) in Eq. (6), it is possible to compute the thread angle required to autocenter an aspheric lens

$$\varphi_{\text{threads}} = 2\tan^{-1}\left[\frac{d_{\text{ring}}}{2\sqrt{\left(\frac{r}{\sin\left\{\tan^{-1}\left[\frac{d}{dr}z(r)\right]\right\}}\right)^2 - Y^2} + 2h + T}\right]. \quad (6)$$

There are two specificities involved in the autocentering of aspheric lenses. The first, which is negligible in most cases, is the radius of curvature variation at the ring to lens interface over the ring decentering range caused by the thread assembly clearance. The second is the decenter and tilt manufacturing error of the aspheric surface to be autocentered with respect to the lens datum axis.

Because of the thread assembly clearance, the actual local radius of curvature at the ring to lens interface is slightly different than the nominal ones used to determine the autocentering thread angle. Also, the radius of curvature at the interface between the ring and the lens is different for diametrically opposite point of contact. Figure 11 shows this concept of the variation of the local radius of curvature for a decentered ring. Figure 11(a) shows the ring decenter at its maximum on the top side of the barrel (maximum position 1 in the figure). For its part, Fig. 11(b) shows the ring decenter at its maximum on the bottom side of the barrel (maximum position 2 in the figure). Because of the optical surface asphericity, the local radius of curvature at the ring maximum position 1 is slightly different than the local radius of curvature at the ring maximum position 2.

It is not straightforward to provide an analytical model to predict the effect of the variation of the radius of curvature over the ring decentering range. However, CAD simulations have been performed for different aspheric surfaces, and the effect of the variation of the radius of curvature has been shown to be negligible. In the example of Fig. 11, the lens diameter is 40 mm and the local radius of curvature interfacing with the ring is 65 mm. For a centering error of the threaded ring of 115 μm, which can be considered to be a typical worst case, the centering error at the center of curvature of the local radius interfacing with the ring is 0.1 μm. This example can be considered as a sensitive

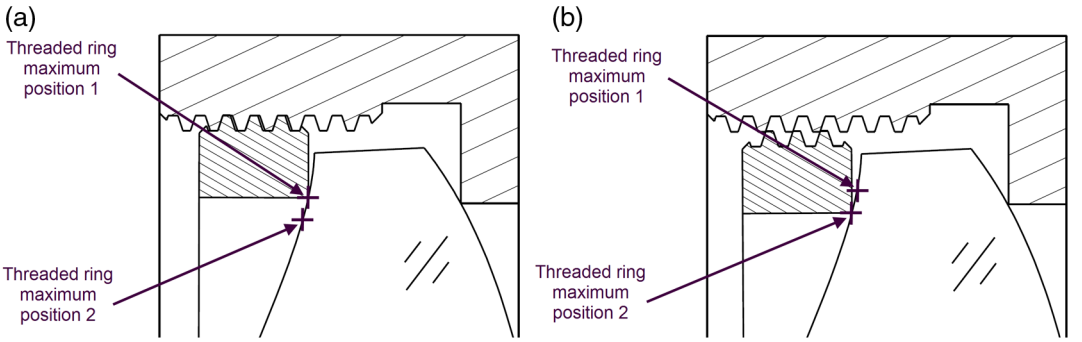

Fig. 11 Ring decentering caused by the thread clearance. (a) Ring decentered at the maximum position 1, (b) ring decentered at the maximum position 2.

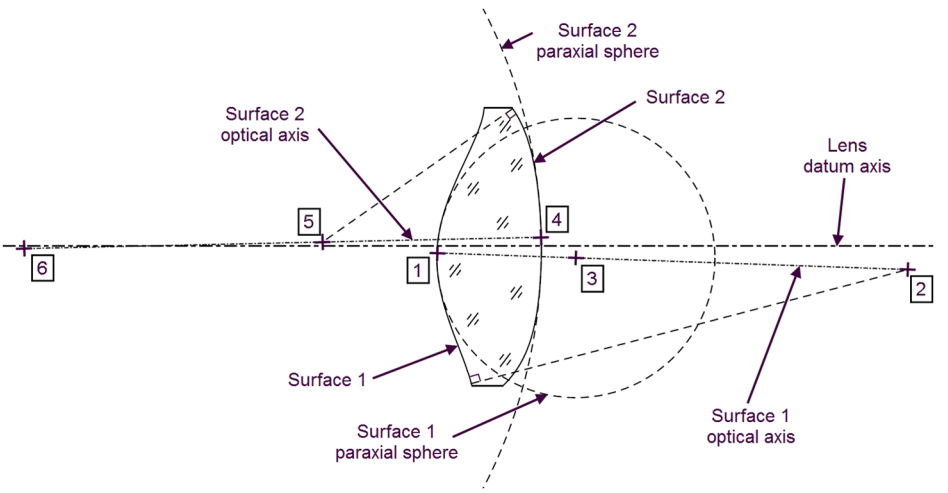

Fig. 12 Biaspheric lens with exaggerated decenter and tilt manufacturing errors.

case as the ring makes contact with the lens at an inflection point where the slope variation is strong.

As mentioned previously, active centering of aspheric lens is generally performed for the surface opposite to the barrel seat by centering the paraxial sphere center of curvature on the barrel reference axis. For autocentering of the aspheric surface, the centering is done at the center of curvature of the local radius interfacing with the ring, rather than at the paraxial sphere center of curvature. For both methods, it is unfortunately impossible to provide a perfect centering because of the decenter and tilt manufacturing errors between the aspheric surface and the optical surface in contact with the barrel seat. Figure 12 shows an example of a lens having two aspheric surfaces. Exaggerated manufacturing errors on decenter and tilt of the aspheric surfaces are shown in the figure. Each aspheric surface is decentered and tilted with respect to the lens reference axis. The point 1 in Fig. 12 corresponds to the aspheric surface 1 center point. The point 2 is the local radius center of curvature at the lens surface 1 mounting interface diameter. The point 3 is the aspheric surface 1 center of curvature of the paraxial sphere. The point 4 corresponds to the aspheric surface 2 center point. The point 5 is the local radius center of curvature at the lens surface 2 mounting interface diameter. Finally, the point 6 is the aspheric surface 2 center of curvature of the paraxial sphere.

Figure 13 shows the lens of Fig. 12 mounted in a lens barrel using the autocentering. The barrel seat constrains the aspheric surface 2 so that the center of curvature of the local radius at the barrel seat interface diameter (point 5) is centered on the barrel reference axis. The threaded ring on the left side of the figure constrains and autocenters the aspheric surface 1 so that the center of curvature of the local radius at the threaded ring interface diameter (point 2) is also centered on the barrel reference axis. The centering errors of the paraxial spheres of both lens surfaces result from the lens manufacturing errors on aspheric surface decenter and tilt with respect to the lens datum axis.

Considering that the centers of curvature of the local radii at the lens mounting interfaces are self-centered, and taking into account the lens manufacturing errors, it is possible to compute the centering error of both paraxial spheres as well as the tilt of the aspheric axes with respect to the barrel reference axis. To do so, we first define a coordinate system origin at the intersection of the lens datum axis and the first optical surface of the lens as shown in Fig. 14.

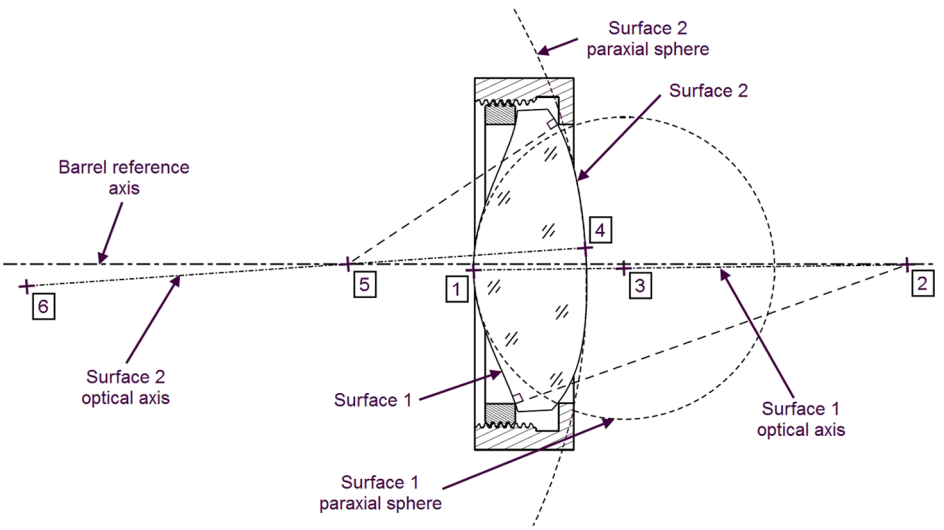

Fig. 13 Autocentered biaspheric lens.

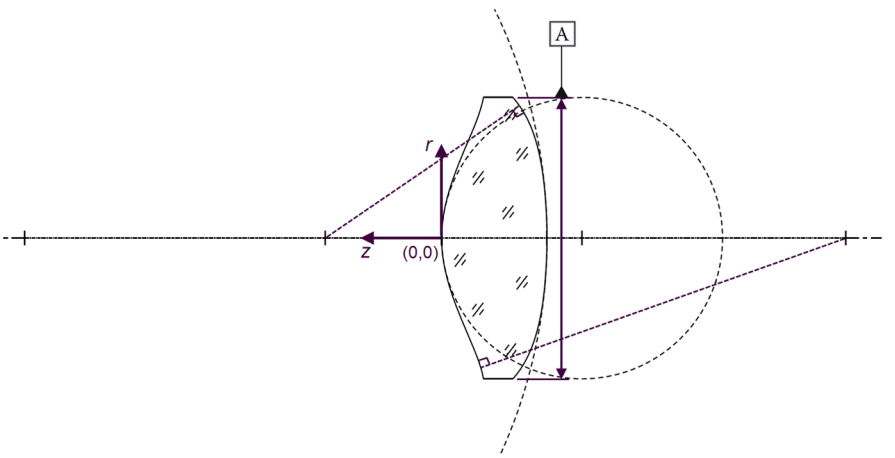

Fig. 14 Biaspheric lens coordinate system.

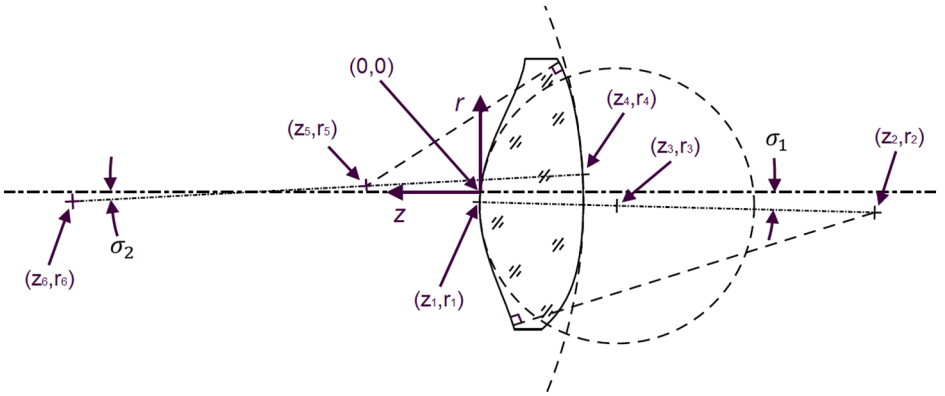

Fig. 15 Biaspheric lens coordinate points.

Then, we need to consider the aspheric lens manufacturing errors. As per ISO 10110 aspheric lens tolerancing, the aspheric surfaces' positioning error results from the tilt manufacturing error σ, and from the lateral displacement L of the center point with respect to the datum axis. As shown in Fig. 15, the position of the aspheric surfaces center points (points 1 and 4), the centers of curvatures of the local radii at the mounting interfaces (points 2 and 5), and the paraxial spheres centers of curvature (points 3 and 6) resulting from the lens manufacturing errors can be defined in terms of Cartesian coordinates with respect to the origin of the coordinate system. The Eq. (7) through Eq. (18) provides the position of each center of curvature in the z- and r-axes of the coordinate system with respect to the origin

$$z_1 = 0, \tag{7}$$

$$r_1 = L_{S1}, \tag{8}$$

$$z_2 = -(R_1 + \Delta z_{S1})\cos(\sigma_1), \tag{9}$$

$$r_2 = r_1 + (R_1 + \Delta z_{S1})\sin(\sigma_1), \tag{10}$$

$$z_3 = -R_2\ \cos(\sigma_1), \tag{11}$$

$$r_3 = r_1 + R_2\ \sin(\sigma_1), \tag{12}$$

$$z_4 \approx -\mathrm{CT}, \tag{13}$$

$$r_4 = L_{S2}, \tag{14}$$

$$z_5 = z_4 + (R_3 + \Delta z_{S2})\cos(\sigma_2), \tag{15}$$

$$r_5 = r_4 - (R_3 + \Delta z_{S2})\sin(\sigma_2), \tag{16}$$

$$z_6 = z_4 + R_4\ \cos(\sigma_2), \tag{17}$$

$$r_6 = r_4 - R_4\ \sin(\sigma_2), \tag{18}$$

where z_1 is the position of the aspheric surface 1 center point (point 1) in the z-axis of the coordinate system, r_1 is the position of the aspheric surface 1 center point (point 1) in the r-axis of the coordinate system, z_2 is the position of the center of curvature of the surface 1 local radius interfacing with the ring (point 2) in the z-axis of the coordinate system, r_2 is the position of the center of curvature of the surface 1 local radius interfacing with the ring (point 2) in the r-axis of the coordinate system, z_3 is the position of the center of curvature of the surface 1 paraxial sphere (point 3) in the z-axis of the coordinate system, r_3 is the position of the center of curvature of the surface 1 paraxial sphere (point 3) in the r-axis of the coordinate system, z_4 is the position of the aspheric surface 2 center point (point 4) in the z-axis of the coordinate system, r_4 is the position of the aspheric surface 2 center point (point 4) in the r-axis of the coordinate system, z_5 is the position of the center of curvature of the surface 2 local radius interfacing with the barrel (point 5) in the z-axis of the coordinate system, r_5 is the position of the center of curvature of the surface 2 local radius interfacing with the barrel (point 5) in the r-axis of the coordinate system, z_6 is the position of the center of curvature of the surface 2 paraxial sphere (point 6) in the z-axis of the coordinate system, r_6 is the position of the center of curvature of the surface 2 paraxial sphere (point 6) in the r-axis of the coordinate system, L_{s1} is the lens manufacturing error on the centering of the aspheric surface 1 with respect to the lens datum axis, L_{s2} is the lens manufacturing error on the centering of the aspheric surface 2 with respect to the lens datum axis, σ_1 is the lens manufacturing error on the tilt of the aspheric surface 1 with respect to the lens datum axis, σ_2 is the lens manufacturing error on the tilt of the aspheric surface 2 with respect to the lens datum axis, R_1 is the surface 1 local radius of curvature at the ring interface, R_2 is the surface 1 paraxial sphere radius of curvature, R_3 is the surface 2 local radius of curvature at the barrel interface, R_4 is the surface 2 paraxial sphere radius of curvature, CT is the lens center thickness, Δz_{s1} is the distance between the surface 1 vertex and the ring interface local radius virtual vertex, and Δz_{s2} is the distance between the surface 2 vertex and the ring interface local radius virtual vertex.

The sign convention used in these equations for the axes tilt angle is shown in Fig. 16. Negative signs have been added in some of the previous equations to be consistent with this sign convention.

Because of radius of the curvature variation in aspheric surface, the distances Δz between the surface vertex and the virtual vertex of the mounting interface local radius of curvature shown in Fig. 17 need to be considered in

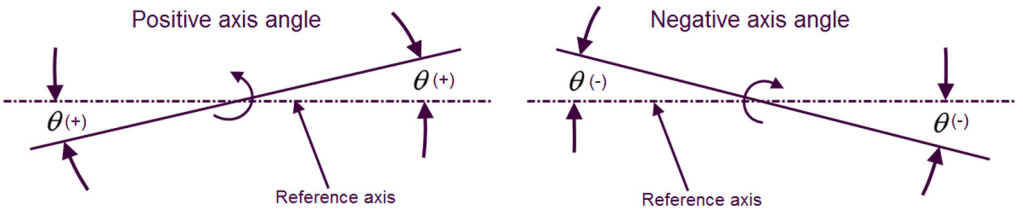

Fig. 16 Aspheric axis tilt sign convention.

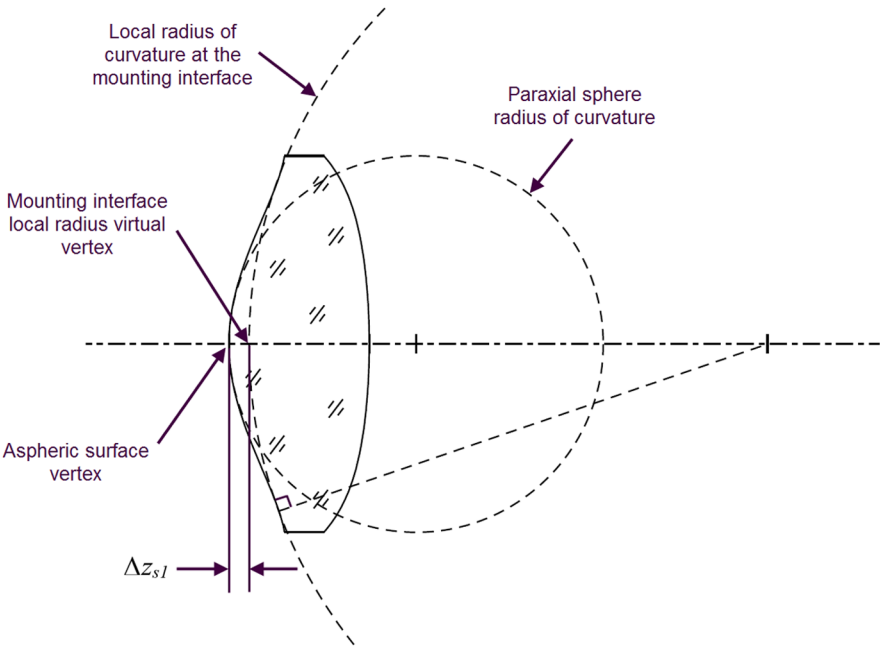

Fig. 17 Distance between the surface 1 vertex and the ring interface local radius virtual vertex.

Eqs. (9), (10), (15), and (16). The distance between the lens mounting interface and the surface vertex can be computed using Eq. (4). Also, the distance between the lens mounting interface and the mounting interface local radius virtual vertex can be calculated using the following sag equation:

$$\text{Sag} = R - \sqrt{R^2 - \left(\frac{D}{2}\right)^2}, \tag{19}$$

where Sag (mm) is the distance from the surface vertex, R (mm) is the mounting interface local radius, and D (mm) is the diameter of the mounting interface at which the sag is calculated.

Finally, the distance Δz is the difference between the distance z from Eq. (4) and the sag from Eq. (19).

The next step is to compute the lens positioning error once mounted in the autocentering mount. Figure 18 shows the lens aspheric surfaces positioning errors from the lens manufacturing prior mounting. Once assembled in the autocentering mount, the axis connecting the centers of curvature of the mounting interfaces radius of curvature (points 2 and 5) becomes coincident with the barrel reference axis as shown in Fig. 19, resulting in a rotation of the lens of the angle θ shown in Fig. 18. Thus, the tilt angles of the aspheric surfaces are given by the following equations:

$$\theta = \tan^{-1}\left(\frac{r_2 - r_5}{z_5 - z_2}\right), \tag{20}$$

$$\theta_1 = \sigma_1 - \theta, \tag{21}$$

$$\theta_2 = \sigma_2 - \theta, \tag{22}$$

where θ is the tilt angle of the axis connecting the local center of curvature of the mounting interface with respect to the barrel reference axis, θ_1 is the tilt angle of the aspheric surface 1 axis with respect to the barrel reference axis, and θ_2 is the tilt angle of the aspheric surface 2 axis with respect to the barrel reference axis.

Using the tilt of the aspheric axes from Eqs. (21) and (22), and considering that the centers of curvature of the mounting interfaces radius of curvature (points 2 and 5) are coincident with the barrel reference axis, it is finally possible to compute the centering error of the aspheric surfaces paraxial spheres with respect to the barrel reference axis with Eqs. (23) and (24)

$$\Delta_{PS1} = -(R_1 + \Delta z_{S1} - R_2)\sin(\theta_1), \tag{23}$$

$$\Delta_{PS2} = (R_3 + \Delta z_{S2} - R_4)\sin(\theta_2), \tag{24}$$

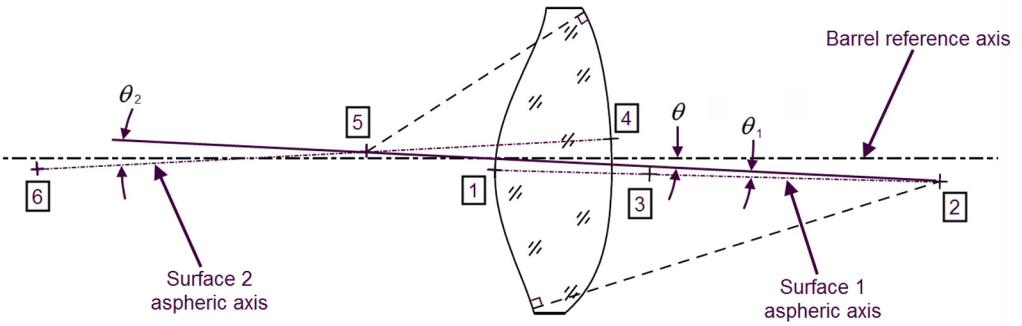

Fig. 18 Biaspheric lens tilt angle parameters.

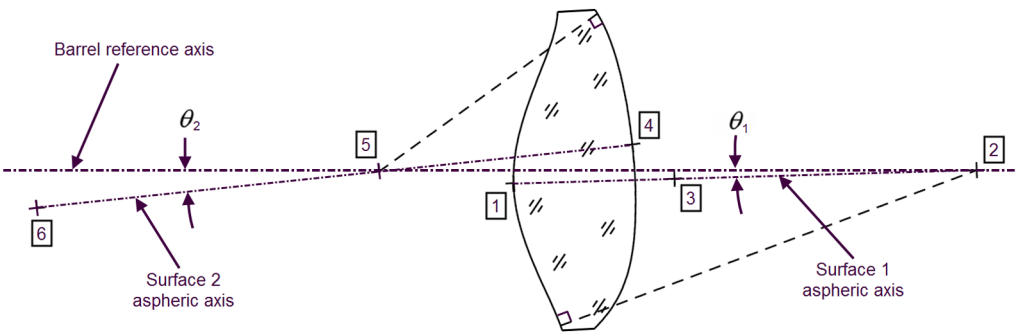

Fig. 19 Tilt angle of aspheric surfaces for an autocentered biaspheric lens.

where Δ_{ps1} is the centering error of the surface 1 paraxial sphere with respect to the barrel reference axis and Δ_{ps2} is the centering error of the surface 2 paraxial sphere with respect to the barrel reference axis.

In the above equations, the radii of convex surfaces are positive, and those of concave surfaces negative.

These equations have been developed for biaspheric lenses. In the case of an aspheric lens having a spherical surface, the same equations are used with the particularity that the same value is used for the local radius of curvature interfacing with the mount, and for the paraxial sphere radius of curvature. For planar surface, these two radii of curvature have an infinite value.

4 Aspheric Lens Autocentering Tests

4.1 *Selected Test Lenses*

Tests have been performed to verify the centering accuracy that can be expected for aspheric lens mounted using the autocentering method.[8] For these tests, two different types of plano-aspheric lenses were considered. Their relevant specifications are summarized in Tables 1 and 2. The first lens type (AHL25-20) has a high asphericity with a maximum deviation from the best-fit-sphere (BFS) of 44 μm. However, the second lens type (ALL25-50) has just a small deviation to the best fit sphere and consequently, a slight change of the local radius of curvature. Both types of lenses have a manufacturing tolerance on the centering error of 5 arc min.

Figure 20 shows the lenses AHL25-20 and ALL25-50 in their respective mounts used for the autocentering tests.

4.2 *Expected Centering Error of Selected Test Lenses*

The effect of the decenter and tilt manufacturing error of the aspheric surface on the autocentering accuracy has been computed for typical manufacturing tolerances of aspheric lenses. For standard precision grade aspheric lens, the tilt between the aspheric surface with respect to the second surface is typically <2.5 arc min, and the lateral displacement of the aspheric surface with respect to the second surface is typically below 30 μm. Using these manufacturing errors,

Table 1 Lens Specifications of chosen test lenses.

Lens designation	Diameter [mm]	Effective focal length [mm]	Radius of curvature [mm]	Clear aperture [mm]	Max. deviation to BFS [μm]	Centering error tolerance [arc min]
AHL25-20	25.0	20.0	15.54	22.5	44.0	5.0
ALL25-50	25.0	50.0	25.56	22.5	8.0	5.0

Table 2 Test lenses aspheric coefficients.

AHL25-20	ALL25-50
$R = 15.54$	$R = 25.56$
$k = -1.35$	$k = -1.01$
$A4 = 2.3618134 \times 10^{-05}$	$A4 = 3.2703958 \times 10^{-06}$
$A6 = -1.1303079 \times 10^{-08}$	$A6 = 7.7205335 \times 10^{-10}$
$A8 = -1.1113906 \times 10^{-11}$	$A8 = 1.6304727 \times 10^{-13}$
$A10 = -2.3981714 \times 10^{-14}$	
$A12 = 3.0357910 \times 10^{-17}$	
$A14 = 1.3660815 \times 10^{-19}$	
$A16 = -1.8881587 \times 10^{-22}$	

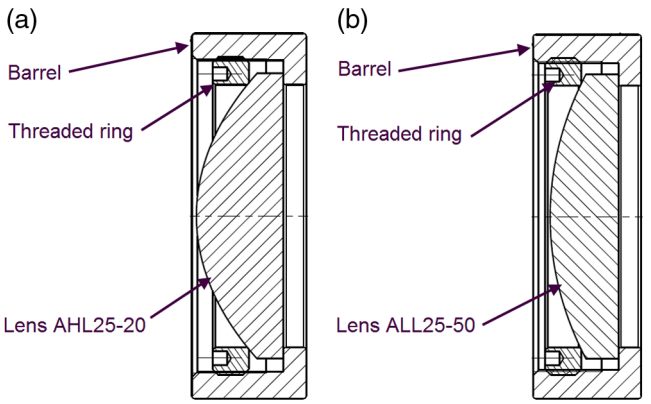

Fig. 20 Mounted aspheric lenses. (a) asphericon lens AHL25-20, (b) asphericon lens ALL25-50.

it is possible to compute the paraxial sphere decenter and the tilt of the aspheric axis. This is done considering the fact that the local radius of curvature of the aspheric surface at the interface with the ring is autocentered on the barrel reference axis as explained previously in the context of Fig. 13. As the second optical surface of the lens is planar, the tilt of the aspheric axis once mounted in the barrel only depends on the tilt manufacturing error between the two optical surfaces, and on the tilt of the barrel seat with respect to the barrel reference axis, which is very small if machined in the same setup as the barrel reference axis. Also, there is no centering error possible between the two optical surfaces because of the planar optical surface of the plano-aspheric lens. Thus, only the tilt error between the two optical surfaces has an influence on the centering of the plano-aspheric lens once mounted in the barrel using the autocentering method. The following table presents the expected contribution of the aspheric surface manufacturing errors on the autocentering accuracy. These values have been computed using Eqs. (7) to (24), which consider the lens geometry and the lens manufacturing errors.

The aspheric surface positioning error values shown in Table 3 are from the aspheric behavior contribution only. Thus, the total aspheric surface centering error is the statistical sum of these values added to the other autocentering contributors that result in a typical centering error of 0.5 arc min for spherical surface. The other autocentering contributors refer to manufacturing tolerance on all the parameters involved in the autocentering condition defined by Eq. (1) as well as geometric manufacturing errors on the threaded ring and barrel. For both lenses, the paraxial sphere centering error once mounted in the autocentering barrel is expected to be around 5 μm with respect to the barrel reference axis.

Table 3 Aspheric surface positioning error caused by the lens manufacturing error for autocentering lens mounting.

Lens designation	Paraxial sphere decenter [μm]	Tilt of the aspheric surface [arc min]
AHL25-20	2.4	2.5
ALL25-50	1.1	2.5

4.3 *Measurement Method*

To begin with the investigation, the production-related deviations of the lenses were measured. For this, the surface form deviation is measured interferometrically and the centering error is measured with a coordinate or form-measuring machine, which will be introduced in more detail now.

To determine the location of the aspheric axis correctly, the surface form deviation is measured as a full surface measurement. This could be done either interferometrically or as a pointwise measurement. To keep measuring time as short as possible, the version discussed below involves an optical distance sensor and a rotational stage with a chuck to hold the lens.[9]

To measure the full surface, the distance sensor is positioned above surface. By rotating the lens, the sensor measures several points on the surface successively. If the sensor keeps its position during the rotation, a circular profile of the surface is detected. To obtain the full surface, the sensor has to detect several circular profiles on different lateral positions. It is also possible to move the sensor continuously along the lateral axis while the lens is rotating. The result then is a spiral profile of the surface. The overall sum of the circular profiles or the spiral profile makes up a point cloud of the measured aspheric surface. Now software can fit the nominal aspheric form into the data by shifting and tilting to reach the lowest surface form deviation value in terms of RMSi defined as the root-mean-square difference between the optical surface under test and the approximating spherical surface. By subtracting the nominal aspheric geometry in its best fitting position to the data, the difference profile reveals the surface form deviation of the manufactured surface. This deviation can be separated into the specific parts of the surface form deviation like power and irregularity that are defined in the DIN ISO 10110-5:2015. Notice, that in this case the surface form deviation does not influence the measurement in a nondeterministic way but is the key clue to determine the aspheric axis correctly. Fitting the nominal aspheric shape to the point cloud data of the measured surface is the most accurate method to determine the position of the surface. The high number of measurement

points included and accounting for the surface form deviation by reaching the lowest RMSi possible provides the best setup in measuring the centering error. Furthermore, both measured errors, i.e., the aspheric surface position and the surface form deviation, have the same origin of coordinates. The determined location of the surface consists of the Cartesian point of the vertex and the direction vector of the axis of symmetry. Both values together are describing properly the definition of the asphere axis. In the next step the relevant geometry parts for the reference, such as lens or mechanical mount datum, have to be measured without losing the origin of coordinates from the surface measurement of the aspheric surface. This allows to get the decenter and the tilt error of the aspheric surface with respect to the reference axis. Thus, now we have come full circle, a coordinate- or form-measuring machine is needed to measure the references within the same coordinate system. Additionally, to see the effect of surface form quality on the centration measurements, each lens type is tested with three different levels of surface form quality including standard quality (SQ), high quality (HQ), and high-end quality, corresponding, respectively, to RMSi tolerance values of 0.30, 0.16, and 0.03 μm.

4.4 *Aspheric Lenses Manufacturing Errors Measurements*

All relevant measurement results of surface form and centering error are shown in Tables 4 and 5. The reference axis for this measurement is defined by the plano-optical surface and the outer rim of the lens. Please notice that the second lens type (ALL25-50) is considered with respect to its best fit sphere due to the small asphericity. As a consequence, the measured aperture is reduced to a small area near the vertex of the surface that can be approximated by the paraxial sphere. Thus, the decenter reported for the lens AHL25-20 corresponds to the centering error of the aspheric surface center point as shown in Fig. 1 as the full aspheric surface can be measured. In the case of the lens ALL25-50, the decenter corresponds to the centering error at the paraxial sphere center of curvature, also shown in Fig. 1, as the asphericity is too small to have accurate measurement of the full aspheric surface.

Table 4 AHL25-20 measurement results for surface form deviation and centering error.

Lens #	RMSi [nm]	RMSΔS [μrad]	Decenter [μm]	Tilt [arc min]
6894 (SQ)	457	321	2.7	1.57
6896 (HQ)	70	90	2.09	0.35
6311 (High-end)	37	45	1.67	2.3

Table 5 ALL25-50 measurement results for surface form deviation and centering error (with respect to best fit sphere).

Lens #	RMSi [nm]	RMSΔS [μrad]	Decenter [μm]
1373 (SQ)	279	236	18.13
1832 (HQ)	114	107	3.35
1306 (High-end)	20	34	9.04

4.5 *Aspheric Lens Autocentering Measurements*

Due to their different shapes, there is one lens mount design for each lens type. Lenses of all three quality levels were inserted into the mount and secured using a threaded ring. The reference axis for measurement is defined as shown in Fig. 21.

4.5.1 *Autocentering mount repeatability measurements*

An important issue is always the repeatability of measurements. For the test in mind the same operator took a measurement series with one measurement object (aspheric lens) in a short period of time. The expectation of such experiment is that the variation of the result data has to be in an acceptable relation to the given tolerance value of the measurement object. During the measurement, all relevant initial conditions between the measurements were reset. Thus, the lens was removed from the chuck of the measurement system and the measurement axes were reset. The results are shown in Table 6.

Another interesting point that should be taken into account is the repeatability of the mounting concept. For this, the same measuring procedure was carried out as for the repeatability of the measuring device but additionally, the lens was taken out of the mount after every single

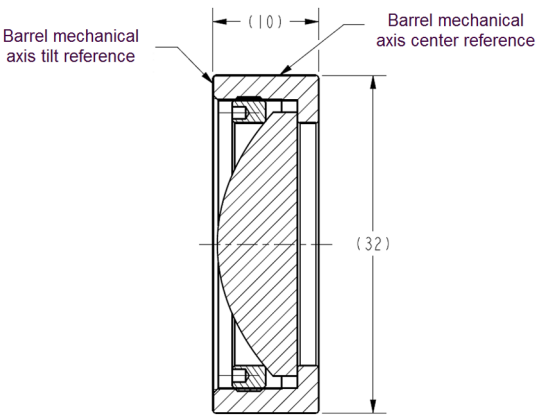

Fig. 21 Definition of reference axis for tilt and decenter measurement.

Table 6 Results of repeatability measurements of measuring device.

	Tilt [arc min]	Decenter [μm]
Measurement #1	5.54	1.38
Measurement #2	5.68	1.42
Measurement #3	5.58	1.37
Mean	5.60	1.39

Table 7 Results of repeatability measurements of the autocentering mount.

	Tilt [arc min]	Decenter [μm]
Measurement #1	0.41	1.86
Measurement #2	0.21	3.66
Measurement #3	0.65	6.05
Measurement #4	0.81	6.89
Measurement #5	0.35	3.27
Mean	0.49	4.35

measurement and was remounted. The lens AHL25-20 #6896 was used for this test and the results are presented in Table 7.

The measurement results of the repeatability measuring device show very small variations: 0.14 arc min of tilt and 0.05 μm of decenter. The variation of the repeatability of the mounting concept is about 0.60 arc min for tilt and 5.03 μm for decenter. The small values for the repeatability of the measuring device confirm that a suitable method was chosen for this investigation, which is perfectly able to detect the state of the mounted lenses.

4.5.2 *Centering error measurements of mounted aspheric lenses*

After determining the repeatability of the measuring device and the mounting concept, both lens mounts were investigated. For this test, one and the same lens was measured in three different mounts for each lens type. Both chosen lenses have the same level of surface quality (standard quality). The results of these measurements are summarized in Table 8. Please notice that the second lens type ALL25-50 was measured with respect to its best-fit-sphere due to its small asphericity. Thus, only the decenter value is listed.

It can be seen from the table that several mounts in combination with one and the same lens result in different centration errors for both lens types. The decenter and tilt variation for the lens AHL25-20 as well as for the lens ALL25-50 are larger than the measuring accuracy of the measuring device and smaller than the repeatability of the mounting concept. So, there is effectively no difference between the three investigated mounts for each lens type and subsequently, a constant centration error of the mounted lenses can be assumed. Thus, for the mounted AHL25-20 a resulting tilt mean of 1.44 arc min and a resulting decentration mean of 7.27 μm were achieved, whereas for the mounted ALL25-50 a resulting decentration mean of 3.73 μm was obtained.

Table 8 Results of decentration measurements comprising the measurement of one lens in three different mounts for each lens type (SQ lens).

	AHL25-20		ALL25-50 (BFS)
Lens mount #	Tilt [arc min]	Decenter [μm]	Decenter [μm]
1	1.34	6.74	5.65
2	1.57	8.01	2.98
3	1.42	7.04	2.55
Mean value	1.44	7.27	3.73

Comparing the centration status of the lenses itself (Tables 4 and 5) and in combination with the lens mount in more detail, some differences in behavior of the two lens types can be obtained. The decentration of the second lens type (ALL25-50), which is treated as a sphere due to small asphericity, is reduced by a factor of 5, which is a considerable improvement. However, it should be mentioned that the centration error measurement of the asphere itself in Table 5 was done with respect to the outer rim. As the outer rim of the lens has no function when mounted using the autocentering, this decenter value of 18.13 μm does not affect the autocentering performance. This shows that for aspheric lens autocentering, the manufacturing tolerance on the centration of the outer rim of the lens with respect to the aspheric surface axis does not influence the centering of the lens once mounted. This contrasts with the standard drop-in method, where the lens rim is used to center the lens in the mount.

Having a closer look at the measuring results of the lens AHL25-20, we can notice that the mean tilt of the mounted lens (1.44 arc min) is very close to the tilt of the aspheric surface with respect to the lens planar surface (1.57 arc min). This is explained by the fact that, for plano-aspheric lenses, the tilt of the aspheric axis once mounted in the barrel only depends on the tilt manufacturing error between the two optical surfaces, and on the tilt of the barrel seat with respect to the barrel reference axis, which is very small if machined in the same setup as the barrel reference axis. As mentioned previously, the decenter reported for the lens AHL25-20 corresponds to the centering error of the aspheric surface center point. As discussed in Sec. 3 and as shown in Fig. 22, the autocentering is performed by centering the local radius center of curvature at the ring interface on the mount reference axis. Because of the distance between this local radius center of curvature and the aspheric surface center point, and because of the tilt error of the aspheric axis with respect to the planar optical surface, the centering error at the aspheric

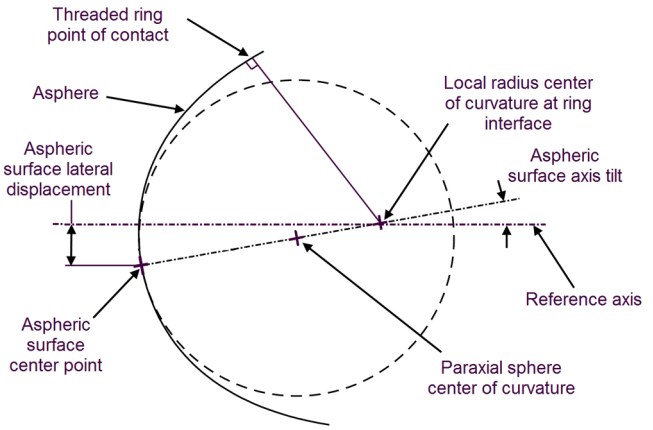

Fig. 22 Aspheric lens decenter at paraxial sphere center of curvature vs aspheric surface center point.

surface center point is amplified compared with the centering error of the paraxial sphere center of curvature. Therefore, the decenter measurements results presented in Table 8 are function of the tilt of the aspheric axis and the local radius of curvature at the threaded ring interface as per: decenter = sin (tilt) * local radius of curvature. For lens AHL25-20, the local radius at the ring interface is 18.39 mm. Considering the measured mean tilt from Table 8, the aspheric surface tilt effect on the centering of the point of rotational symmetry is sin (1.44 arc min) * 18.39 mm = 7.7 μm, which is very close to the mean decenter measured of 7.27 μm.

For comparison purposes, Table 9 shows the decenter error of the paraxial sphere for the lens AHL25-20. As aspheric lenses are most of the time centered by aligning the paraxial sphere center of curvature on the barrel reference axis, the measurement results of Table 9 are more relevant for a comparison purpose between active alignment and the autocentering method.

A further investigation deals with the effect of the different surface quality levels on the minimum achievable centration error of the mounted lenses. Lenses of three different levels of surface form quality (SQ, HQ, and high-end quality) were inserted into one lens mount and measured (again for each lens type). The results are summarized in Table 10. Once again, please notice that the second lens type ALL25-50 was measured with respect to its best-fit-sphere due to its small asphericity. Thus, only the decenter value is listed.

Having a look at the results of the mounted AHL25-20 first, it can be seen that the tilt errors of the mounted lenses are very close to the tilt errors between the two optical surfaces of each lens as shown in Table 4, which is exactly what was expected. The decenter, which is the decenter at the point of rotational symetry, is a function of the tilt and also includes variation from the repeatablility of the mounting concept. For the high-quality lens, significant lower values for decenter were measured. This is because of the small tilt error between the two optical surfaces (0.35 arc min). Because of the repeatability of the mount, there is no correlation that can be done between the surface quality of the lens and the measured centration errors. Thus, the surface quality effect on the lens autocentering precision can be considered to be negligible compared with the repeatability.

The decenter values for lens ALL25-50 are considered with respect to their centering errors when they were unmounted (Table 5). As mentioned previously, the lens rim centering error does not affect the position of the lens once mounted in the barrel as the autocentering uses surface contact mounting. Therefore, there is no relationship between the centering error of Tables 5 and 10, but significant centering improvement can be observed for SQ and high-end lens that have a larger centering error between the aspheric surface and the lens rim. The measurement results of the mounted ALL25-50 show differences between the consecutive quality levels smaller than the repeatability of the mounting concept. Although the centering error of the high-end quality lens is 3.45 μm smaller than the SQ lens, it is difficult to conclude that the surface quality has a significant influence on the centering error because of the repeatability of the mount.

Table 9 Results of decentration measurements of the paraxial sphere of lens AHL25-20 comprising the measurement of one lens in three different mounts (SQ lens).

	AHL25-20 (BFS)
Lens mount #	Decenter [μm]
1	1.71
2	1.99
3	1.69
Mean value	1.80

Table 10 Results of decentration measurements of a lens with three levels of surface form quality in one and the same lens mount for each lens type.

	Lens mount #1		Lens mount #1	
AHL25-20 lens quality	Tilt [arc min]	Decenter [μm]	ALL25-50 lens quality	Decenter [μm]
SQ	1.34	6.74	SQ	5.65
HQ	0.41	1.86	HQ	4.48
High-end	2.11	8.57	High-end	2.20

Table 11 Summary of the centering error measurements of aspheric lenses mounted using autocentering.

	AHL25-20			ALL25-50 (BFS)
Lens mount #	Tilt [arc min]	Decenter [μm] (center point)	Decenter [μm] (paraxial sphere)	Decenter [μm] (paraxial sphere)
Mean	1.40	6.63	1.80	3.82
SD	0.37	1.96	0.73	2.04

4.5.3 *Centering error measurements summary*

The previous sections present measurement results on unmounted lenses, repeatability of the centering error measurement method, repeatability of the autocentering method, the centering variability from one mount to the other, and the centering variability for different lens surface form quality. Table 11 summarizes these measurements by giving the mean and the SD from all the measurements performed.

5 Conclusion

This paper discussed the specificities of aspheric lens for mounting and alignment. It described how the lens manufacturing error affects the positioning error of an aspheric lens once mounted in a barrel. Typical mounting and alignment methods for aspheric lens were also presented. Finally, a novel method to mount and align aspheric lenses using the autocentering principle has been discussed. Centering measurement results for different aspheric lenses mounted using the autocentering were presented. The results of the study performed in this paper show that this new lens mounting method for aspheres provides a simple and an accurate

mounting method that bridges the advantages of the standard drop-in and the active alignment.

References

1. ISO 10110-6, *Preparation of Drawings for Optical Elements and Systems–Part 6: Centering Tolerances*, ISO central Secretariat, Geneva, Switzerland (2015).
2. ISO 10110-12, *Preparation of Drawings for Optical Elements and Systems–Part 12: Aspheric Surfaces*, ISO central Secretariat, Geneva, Switzerland (2007).
3. M. Trabert, U. Fuchs, and S. R. Kiontke, "Asphere wedge decenter: what you see is not always what you get," *Proc. SPIE* **9951**, 99510I (2016).
4. F. Lamontagne et al., "Lens auto-centering," *Proc. SPIE* **9626**, 962619 (2015).
5. F. Lamontagne et al., "Disruptive advancement in precision lens mounting," *Proc. SPIE* **9582**, 95820D (2015).
6. F. Lamontagne, *Chapter 7: Optomechanical Tolerancing and Error Budgets, Handbook of Optomechanical Engineering*, 2nd ed., CRC Press, Boca Raton, Florida (2017).
7. P. R. Yoder, Jr. and F. Lamontagne, *Chapter 8: Optical Mounts: Lenses, Windows, Small Mirrors, and Prisms, in Handbook of Optomechanical Engineering*, 2nd ed., CRC Press, Boca Raton, Florida (2017).
8. F. Lamontagne et al., "Aspheric lens mounting," *Proc. SPIE* **10590**, 1059025 (2017).
9. J. Heinisch and E. Dumitrscu, "Method and device for determining the position of the symmetrical axis of an aspherical lens surface," EU Patent EP1918687 A1 (2006).

Frédéric Lamontagne is a senior optomechanical engineer at the National Optics Institute (INO) in Canada. With over 15 years of professional experience, he has been involved in several projects for astronomy, space, military, medical, and commercial applications. Over the past few years, he has performed a comprehensive study on the interaction between lenses and mounts, and on optomechanical tolerance analysis. He has authored and co-authored 15 technical papers, and has 7 awarded and pending patents.

Ulrike Fuchs started her academic career in 2003 working on numerical simulations for ultrashort pulse propagation in optical system. Joining asphericon in 2010 as an optical designer shifted her research focus to interlinking manufacturing of aspherics and metrology with questions in optical design. She is continuously working on concepts that allow a prediction of system performance during optical design and tolerancing processes. Recently, great emphasis is put on transferring those ideas to freeform optics.

Martin Trabert studied laser and opto-technology (B. Eng degree) at the University of Applied Science in Jena. He joined asphericon in 2015 for his bachelor's thesis, in which he evaluated an autocollimated measurement system for the centration measurement of aspheric lenses and has also developed a new approach by measuring the full surface of the aspheric lens. Since then, he has worked at asphericon's metrology department and is responsible for extended measurements of optical and opto-mechanical components.

Anna Möhl studied laser and opto-technology (B. Eng. and M. Eng. degrees) at the University of Applied Sciences in Jena. In 2015, she joined asphericon for her master's thesis in the optical design department. In the scope of her master's thesis, she designed a compact refractive Gauss to Top-Hat beam shaping system. Currently, she is working as an optical designer, developing optical designs for R&D projects as well as customized lenses or systems.